Preliminary Hydraulic Design and Test of A Centrifugal Blood Pump

Maruay Anansukkasam, Rumpa Chaijinda, and Asi Bunyajitradulya*

Department of Mechanical Engineering, Faculty of Engineering, Chulalongkorn University
Bangkok 10330, Thailand
* Corresponding Author: Tel: 02 218 6645, Fax: 02 218 6645, E-mail: asi.b@chula.ac.th

Abstract

The paper presents the design scheme and considerations for the preliminary hydraulic design of a centrifugal blood pump, the evaluation of the design via model testing, and finally the more realistic prediction of the prototype performance parameters based on the results of the model testing. The design is based on 'one-dimensional' Euler's turbomachine equations and the design speed of 1,000 RPM, together with heart parameters, and some blood trauma and mechanical considerations. A 2X scale-up model is subsequently constructed and tested. The initial test of the model shows that the pump cannot achieve the prototype-equivalent desired head-flow at the design speed. Subsequently, a series of additional model tests are performed, and the result shows that the characteristic dimensionless head-flow curve of this pump, $C_H = -5{,}423C_Q^2 + 20.66C_Q + 0.1615$, is Reynolds number (Re) independent over the range of Re tested of 1.4-2.9x10^6, yet still 10 times higher than the prototype Re of 1.2x10^5. Similarity scaling, based on the Re-independent assumption of the newly acquired dimensionless head-flow curve, is then used to predict the required operating speed of the prototype, 1,185 RPM, approximately 20% above the design value. Additional test at this RPM confirms the prediction and shows that the model pump can successfully achieve the prototype-equivalent head-flow at this speed. The more realistic performance parameters of the prototype, based on the results of the model testing, are then predicted. It is subsequently concluded that, if the dimensionless head-flow curve of this pump is independent of Re down to the prototype Re, the prototype should be able to deliver the desired head-flow successfully at 1,185 RPM. The remaining issue is then whether the assumption of Re independence down to the prototype Re is valid.

Keywords: centrifugal blood pump, ventricular assist device, VAD, hydraulic design, pump test

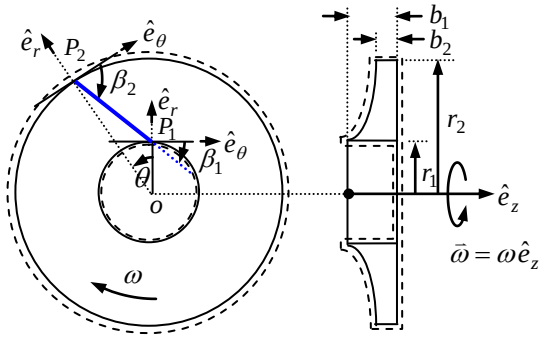

Fig. 1. Control volume and notations for geometric variables.

$\theta, \hat{e}_\theta$ = tangential direction and tangential unit vector, positive in the direction of U; also, blade subtended angle

$r, \hat{e}_r$ = radial direction (and radius) and radial unit vector, positive away from the center

V = absolute fluid velocity

U = blade peripheral velocity

β = blade angle, measured from $\hat{e}_\theta$ and away from $\hat{e}_r$

α = angle of absolute fluid velocity V, measured from $\hat{e}_r$ and towards $\hat{e}_\theta$

N = rotational speed

ω = impeller angular velocity

d = impeller diameter

b = impeller width

$\lambda_d := d_1 / d_2$

$\lambda_b := b_1 / b_2$

subscripts

1,2 = impeller inlet and exit, respectively

m, p = model, prototype

$:=$ = equal by definition

Other notations are given in the text.

1. Introduction

A blood pump, or ventricular assist device (VAD), is a medical device that is used for assisting the function of the heart in pumping blood in heart disease patients. Commercially, the approved VADs are available from a few companies [e.g., 1-3]. Presently, though, they need to be imported at high cost and the local availability is still rare even for the imports. This initiates the present preliminary design and test project.

Naturally, there are many aspects in the design and development of a VAD, for example, fluid dynamics, rotor dynamics, strength and wear, drive, and blood trauma. However, here we focus primarily on the hydraulic design.

The objective of the paper is to present our design scheme and considerations for the preliminary design of a (centrifugal) blood pump and to present the evaluation of our design scheme via the result of the model testing. In the design process, the heart parameters and, to the first-order, the blood trauma, especially hemolysis, is considered. The design is based on 'one-dimensional' Euler's turbomachine equations. The result of the design is evaluated for the pump performance by the testing of a 2X scale-up model. While the hemolysis is preliminarily considered in the design process, it is, however, not yet tested.

2. Design Specification Parameters

The fluid is blood with density of 1,050 kg/m^3 and dynamic viscosity of 4x10^{-3} pascal-second. The design flowrate and head correspond to the rest state (designated A) with blood volume flowrate of Q_A = 5.8 L/min and mean arterial pressure H_A = 93 mmHg [4]. Note that at exercise state (designated B), Q_B = 25.5 L/min and H_B = 110 mmHg. At present, we target the design at the rest state A.

3. Pump Design

The current hydraulic design process can be divided into 3 major steps: pump type selection, impeller design, and casing design.

3.1. Pump Type Selection

For the appropriate pump type, we consider the dimensionless specific speed ω_s, defined by $\omega_s := \omega\sqrt{Q}/(gH)^{3/4}$, where ω is the angular velocity (rad/s), Q is volume flowrate (m^3/s), and H is total hydraulic head (m). While we have some degree of freedom in choosing the design rotational speed and consequently the type of machine (i.e., radial-flow vs axial-flow), in order to avoid the complications of wear and drive we target the design rotational speed in the typically low range of 1,000-4,000 RPM and choose the design rotational speed at 1,000 RPM. Taking into account the design point A, this results in ω_s of 0.16-0.65, which fall in the radial-flow type range [5-6] and we choose to design a radial-flow machine. Note that if we choose instead a higher target range of rotational speed in the order of a few ten thousands RPM, this will result in an axial-flow type machine.

3.2. Impeller Design

For the impeller design, we use the control volume as shown in Fig. 1 and follow the set of Euler's turbomachine equations, with the target design point at the rest state (A) and with the following assumptions:

- radial-entry flow ($\alpha_1 = 0$)
- shockless entry/exit condition (relative fluid velocity with respect to the rotating blade is tangent to the blade angle at inlet and exit)
- straight blade
- constant absolute radial velocity along the blade passage
- neglect all losses.

The notations for geometric variables are given in Notations and Fig. 1.

Design Scheme and Analysis

Our design scheme can be summarized with Eq. (1),

$$K := \frac{\Delta p_A}{Q_A \omega_A} = \Psi \frac{\rho}{2\pi b_1}, \qquad (1)$$

where

$$\Psi := \left[\left(\frac{1}{\lambda_d^2} - 1\right)\tan\alpha_1 + \frac{1}{\lambda_d^2 \tan\beta_1} - \frac{\lambda_b}{\tan\beta_2}\right] \qquad (2)$$

is the parameter that is a function of the geometries of the machine ($\beta_1, \beta_2, \lambda_d, \lambda_b$) and the flow ($\alpha_1$). Specifically, we cast the combination (K) of the *design specification parameters* Δp, Q, and ω (at the design point A) in terms of the *dimensionless* and *dimensional design geometric variables* $\beta_1, \beta_2, \lambda_d, \lambda_b, \alpha_1$, and b_1, respectively, and the fluid density ρ. As a result, $K := \Delta p_A/(Q_A \omega_A)$ is a constant. Note that Eq. (1) can be derived from the set of Euler's turbomachine equations, which can be cast in terms of the geometric variables as follows.

The velocity triangle relations:

$$V_i = \frac{\sin\beta_i}{\cos(\alpha_i - \beta_i)} U_i,$$

$$V_{i\theta} = \frac{\sin\alpha_i \sin\beta_i}{\cos(\alpha_i - \beta_i)} U_i,$$

$$V_{ir} = \frac{\cos\alpha_i \sin\beta_i}{\cos(\alpha_i - \beta_i)} U_i, \qquad (3)$$

where i is 1 or 2, the inlet or exit cross section.

Conservation of mass:

$$\frac{V_{2r}}{V_{1r}} = \lambda_d \lambda_b. \qquad (4)$$

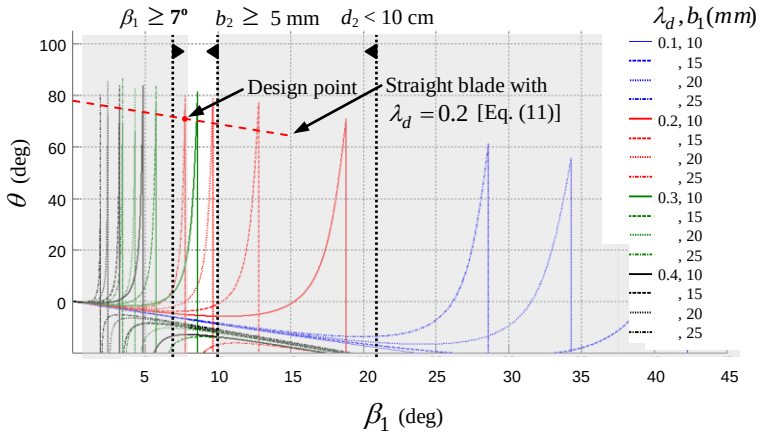

Fig. 2. The design chart: the relation for $\theta(\beta_1; \lambda_d, b_1)$.

Volume flowrate:

$$Q = 2\pi \frac{\tan\beta_1}{1+\tan\alpha_1 \tan\beta_1} b_1 \omega r_1^2 . \quad (5)$$

Euler's hydraulic torque $T_h = \dot{m}(r_2 V_{2\theta} - r_1 V_{1\theta})$:

$$T_h = \Psi \left(\frac{\tan\beta_1}{1+\tan\alpha_1 \tan\beta_1} \right)^2 2\pi\rho b_1 \omega^2 r_1^4 . \quad (6)$$

Hydraulic power ($\dot{m}gH_p = T_h\omega$):

$$\dot{m}gH_p = \Psi \left(\frac{\tan\beta_1}{1+\tan\alpha_1 \tan\beta_1} \right)^2 2\pi\rho b_1 \omega^3 r_1^4 . \quad (7)$$

Hydraulic head:

$$H = \frac{1}{g} \Psi \left(\frac{\tan\beta_1}{1+\tan\alpha_1 \tan\beta_1} \right) \omega^2 r_1^2 . \quad (8)$$

Static pressure rise (neglect kinetic and potential head):

$$\Delta p = \Psi \left(\frac{\tan\beta_1}{1+\tan\alpha_1 \tan\beta_1} \right) \rho \omega^2 r_1^2 . \quad (9)$$

For simplicity, we choose to design straight-blades. Thus, we have the following additional relations:

Geometric relations for straight blade:

$$\beta_2 - \beta_1 = \theta \quad (10)$$

and, according to the sine law for the triangle oP_1P_2 in Fig. 1,

$$\theta = 90^o - \beta_1 - \arcsin\left(\lambda_d \sin(90^o + \beta_1)\right). \quad (11)$$

In order to reduce the potential of flow separation in the blade passage, we choose the scheme of constant absolute radial velocity V_r, which is equivalent to constant relative radial velocity with respect to the rotating blade. Therefore, we have

$$\lambda_d \lambda_b = 1 \quad \text{and} \quad rb = r_1 b_1 \quad (12)$$

and the blade width profile:

$$b(r) = \frac{Q}{2\pi r V_r} . \quad (13)$$

With the assumption of radial-flow entry ($\alpha_1 = 0$), and the conditions of straight blade ($\beta_2 - \beta_1 = \theta$) and constant absolute radial velocity ($\lambda_d \lambda_b = 1$), we can rewrite Eq. (1) as

$$\theta = \tan^{-1}\left(\frac{\lambda_d \tan\beta_1}{1 - 2\pi(Kb_1/\rho)\lambda_d^2 \tan\beta_1} \right) - \beta_1 , \quad (14)$$

where $\theta(\beta_1 ; \lambda_d, b_1 ; K)$. Here, the two semicolons are used to differentiate what we consider independent variables, variable parameters, and constant parameters, respectively.

For a given fluid (ρ), Eq. (14) is the relation for the blade subtended angle θ in terms of the dimensionless design geometric variables β_1 and λ_d, the dimensional design geometric variable b_1, and the design specification parameter K. Choosing β_1 as the variable, and λ_d and b_1 as the parameters, we can plot this relation as shown for the ranges of λ_d = 0.1 –

0.4 and b_1 = 10 – 25 mm in Fig. 2. Figure 2 is then used as a design chart. Note that all points on the lines on this chart correspond to the same value of the design specification parameter K.

Design Constraints and The Design Solution

In order to choose the suitable design solution, we impose further constraints on the design solutions on the chart (Fig. 2) as follows.

- Manufacturing limitation, $\beta_1 \geq 7^\circ$: Therefore, most of the black lines (λ_d = 0.4) in Fig. 2 are not suitable.
- Size limitation, d_2 < 10 cm: For a typical blood pump, the inlet diameter is in the order of 1 cm. If we choose λ_d = 0.1, this will make d_2 = 10 cm, not yet including the casing. The blue lines (λ_d = 0.1) are therefore considered not suitable.
- Exit blade width limitation, $b_2 \geq$ 5 mm: The remaining solutions are the solid green $\lambda_d, b_1(mm)$ = (0.3,10) and the remaining reds $\lambda_d, b_1(mm)$ = (0.2,10-25). Since $\lambda_b = 1/\lambda_d$, the solid green (λ_b = 3.33) with b_1 = 10 mm and the reds (λ_b = 5) with b_1 = 10-20 mm will give b_2 < 5 mm, these are therefore considered not suitable.
- As a result, we are left with the one that we consider suitable under the constraints to be the dashed-dotted red line, i.e., $\lambda_d, b_1(mm)$ = 0.2, 25 mm.
- The solution: While all points on this line satisfy the specified K and the foregoing assumptions, not all points on this line satisfy the condition of straight blade. Specifically, for a straight blade, we also have the geometric relation Eq. (11). Thus, for a given λ_d of 0.2, we find the solution on the line $\lambda_d, b_1(mm)$ = 0.2, 25 to be β_1 = 7.73° and θ = 70.84°.
- Finally, β_2 can be determined from Eq. (10), r_1 from Eq. (5), V_{1r} from Eq. (13) evaluated at inlet 1, and blade width profile $b(r)$ also from Eq. (13) with constant $V_r = V_{1r}$ and Q. Table 1 summarizes the geometric variables for the prototype, and Table 2 at the back summarizes important performance parameters for the design of the prototype (in comparison to those of the model test results). Note that this is a backward, straight blades impeller.

Table 1. The geometry of the impeller.

Geometric Variables				
β_1 (deg)	7.73°		β_2 (deg)	78.57°
d_1 (mm)	13.16		d_2 (mm)	65.80
b_1 (mm)	25		b_2 (mm)	5
λ_d	0.2		λ_b	5
θ (deg)	70.84		-	-

The Question of The Number of Blades

With the blade shape determined, the issue of the appropriate number of blades and blade thickness, which are related to flow quality, blockage effect at impeller inlet, and mechanical strength, remain. At present, the issue is not yet fully addressed, and we plan to address the issue more elaborately in the future. On the other hand, since we set out to test this design with a *model* made from acrylic for future flow measurement and observation, giving the priority to the mechanical strength, we determine the required blade thickness to be 1.5 mm. Subsequently, considering and avoiding excessive blockage effect, we decide on six blades. This results in the blockage ratio at the impeller inlet diameter of 2.9%. Here, blockage

ratio is defined as the total radial area blocked to the total radial area, $B = nt\sin\beta_1/(\pi d_1)$, where n is the number of blades and t is the blade thickness. Note that for a future *prototype*, which will be made from a more suitable material, the restriction from the blade thickness is expected to be less severe; and, thus less blockage.

Predicted Off-Design Head-Flow Curve of The Prototype at Constant RPM

In order to predict the off-design head-flow curve of the prototype at constant RPM, we cannot use the design relations (5)-(9) since they are restricted to shockless entry/exit condition of the velocity diagrams. Instead, we need to employ the original Euler's torque and hydraulic head equations, $T_h = \dot{m} r_2 V_{2\theta}$ ($V_{1\theta}$ = 0) and $H = (\dot{m} g H)/\dot{m} g = T_h \omega/\dot{m} g = U_2 V_{2\theta}/g$. Solve $V_{2\theta}$ from the velocity diagram, we have $V_{2\theta} = U_2 - V_{2r}\cot\beta_2$. Rewrite V_{2r} in terms of Q [Eq. (13)] and substitute the resulting $V_{2\theta}$ in terms of Q into the equation for H above, we finally have

$$H = -\left(\frac{U_2 \cot\beta_2}{\pi d_2 b_2 g}\right)Q + \frac{U_2^2}{g}. \qquad (15)$$

The resulting ideal dimensional head-flow curve for the prototype from Eq. (15) is shown later in Fig. 5, together with the model test result. Briefly, we see that the ideal head decreases linearly and slowly with the flow, according to the slope $-(U_2\cot\beta_2)/(\pi d_2 b_2 g)$. Note that the slope of Eq. (15) can be used as a guide in the design of the characteristic slope of the dimensional head-flow curve of the pump.

If we define the dimensionless head C_H as $C_H := gH/\omega^2 d^2$, the dimensionless flow C_Q as $C_Q := Q/\omega d^3$, and the Reynolds number Re as $\mathrm{Re} := \omega d^2/\nu$, where d_2 is chosen for the characteristic diameter d, Eq. (15) can be rewritten as

$$C_H = -\left(\frac{d_2 \cot\beta_2}{2\pi b_2}\right)C_Q + \frac{1}{4}. \qquad (16)$$

The resulting ideal dimensionless head-flow curve for the pump from Eq. (16) is shown later in Fig. 6, together with the model test result. Again, C_H varies linearly and slowly with C_Q, according to the slope $-d_2\cot\beta_2/(2\pi b_2)$. Note that this slope, unlike its dimensional counterpart which still depends on the velocity U_2, depends on geometric variables alone. Similar to Eq. (15), the slope of Eq. (16) can be used as a guide in the design of the characteristic slope of the dimensionless head-flow curve of the pump.

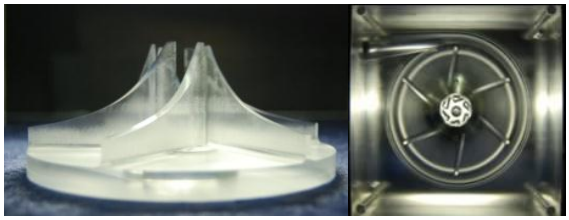

(a) (b)

Fig. 3. The 2X scale-up model: (a) impeller, (b) assembly of the impeller and the pump casing.

3.3. Casing Design

For the volute shape, with similar reason as the blade passage, in order to reduce the potential of flow separation we choose the scheme of constant tangential velocity throughout the volute passage. Preliminarily, we also consider the hemolysis. Yamane et al. [7-8] suggest that the suitable shear rate should be below 100,000 sec^{-1}. Since the maximum shear rate potentially occurs at the gap between the rotating impeller and the casing at the volute

inlet, we choose the gap width to be 1.5 mm; resulting in the shear rate at this location of 2,300 sec^{-1}. At this point, it is important to note that hemolysis is related to the local shear and therefore can occur at the location where the local shear is high. Thus, the current consideration is only to the first-order.

4. Model, Similarity Scaling, Model Testing

Model

In order to evaluate the performance of the current design, we choose to make a 2X scale-up model, made from acrylic, for ease of future flow observation and measurement. Figure 3 shows the resulting 2x scale-up model, which is the result of the current design scheme. Note that the volute passage cross section is rectangular. In order to fit to a 1-inch pipe, we design a diffuser that changes the rectangular cross section to 1-inch diameter circular cross section.

Similarity Scaling Law

In scaling, we employ similarity scaling law

$$C_H = f\left(C_Q, \mathrm{Re}\right), \qquad (17)$$

where the head and flow coefficients, and the Reynolds number is defined in Sec. 3.2.

The Question of Reynolds Number

To strictly follow this similarity law, the Reynolds number must be taken into account. The design prototype Reynolds number at A is calculated to be 1.2×10^5. Given the 2X scale-up model, this can be done either by, for example,

- using glycerine-water solution in order to get the kinematic viscosity of the blood so that the model can be run at reasonable speed ($N_m = N_p/4$) but the head will be relatively low ($H_m = H_p/4$), or

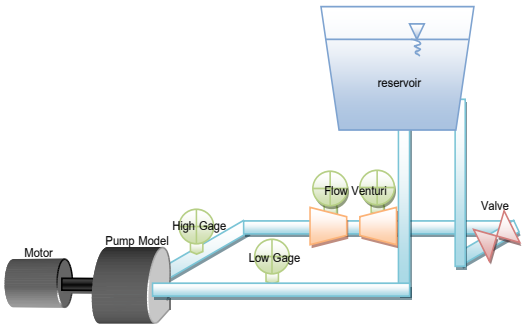

Fig. 4. Schematic diagram of the pump test rig.

- using water (ν_{blood}/ν_{water} = 4.7), but the test speed and the head will both be very low, $N_m \sim N_p/20$ and $H_m \sim H_p/100$.

At this stage, we decide to first neglect the effect of Re, i.e., $C_H = f(C_Q)$, use water as working fluid, and run the model at the same design speed as for the prototype, i.e., 1,000 RPM, for ease of measurement. This corresponds to Re of 2.3×10^6, approximately 20 times higher than that of the prototype. The effect of Re will be partially addressed in this work but will be addressed in more detail in the future. Thus, we have the scaling laws between the model and the prototype as

$$\frac{Q_m}{Q_p} = 8\left(\frac{N_m}{N_p}\right) \quad \text{and} \quad \frac{H_m}{H_p} = 4\left(\frac{N_m}{N_p}\right)^2. \qquad (18)$$

Finally, in this work we choose to test the model and deduce the performance of the prototype from the scaling law at equal speed. Thus, we have the scaling laws, from Eq. (18),

$$\frac{Q_m}{Q_p} = 8 \quad \text{and} \quad \frac{H_m}{H_p} = 4. \qquad (19)$$

Model Pump Testing

Figure 4 shows the schematic diagram of the test rig. Briefly, it is a closed loop test rig with upper reservoir open to atmosphere. Two pressure gauges are installed at 20 pipe diameters away from the pump inlet and exit for

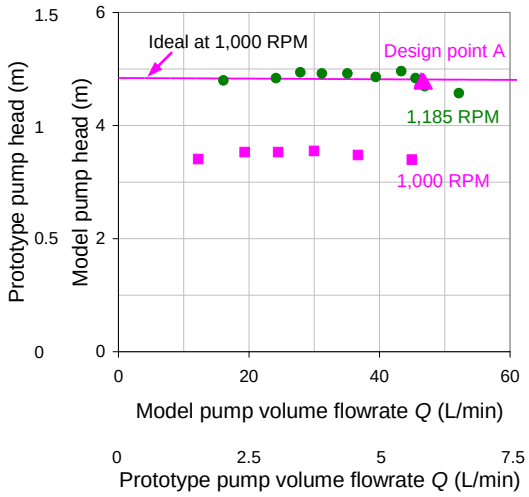

Fig. 5. Dimensional head-flow curves for the model and the prototype.

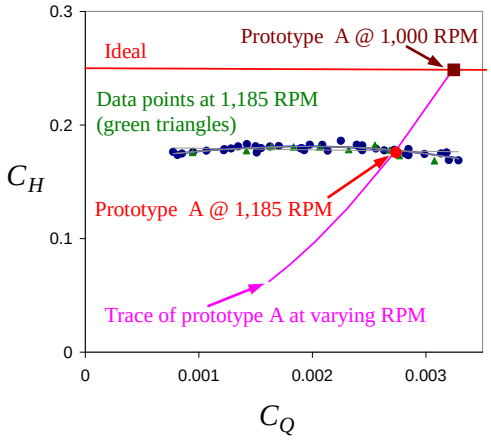

Fig. 6. Dimensionless head-flow curve from model testing and the prediction of the operating speed of the prototype.

the measurement of static pressures. Volume flowrate is measured by a venturi.

The total hydraulic head is determined from

$$H = \left(\frac{p}{\rho g} + \frac{\alpha \bar{V}^2}{2g} + z \right)_2 - \left(\frac{p}{\rho g} + \frac{\alpha \bar{V}^2}{2g} + z \right)_1 , \quad (20)$$

where, because of equal inlet and exit pipe diameters, the kinetic heads cancel and the reading of the pressure gages is corrected for the elevation. Overall, the total hydraulic head depends essentially on the static pressure rise across the pump.

5. Model Pump Test Results

Dimensional Performance

The model pump test result is shown in Fig. 5. Presently, we test the pump at 1,000 RPM. Focus first on the data points at 1,000 RPM; the data points at 1,185 RPM will be explained later in Sec. 7. The result shows that the head changes relatively little with the flow over the test range (the variation is approximately 4% of the average value, and well within the uncertainty of measurement), qualitatively in agreement with the ideal head-flow curves from Eq. (15). At the same volume flowrate, the actual total hydraulic head is about 70% of the ideal value in the test range. Although not shown, since the head is approximately constant, the hydraulic power (= $\dot{m}gH$) naturally increases with the volume flowrate. The maximum efficiency (η) at this speed is found to be 29.8%.

Effect of Re and Dimensionless Performance

In order to get some preliminary information on the effect of Reynolds number, we make additional tests to a total of 7 speeds, evenly spaced from 600 – 1,100 RPM or Re from 1.4-2.5x10^6. Figure 6 shows the scatter plot of the head against the flow coefficients of all data points. Disregard first the data points at 1,185 RPM in the figure; they are not included in the present analysis. The uncertainties of both C_Q and C_H are estimated to be $\pm 10\%$ of the reading value. Firstly, the result shows that the dimensionless head-flow curve is in qualitative agreement with the ideal one, C_H varies slowly with C_Q. More importantly, the result suggests that the effect of Reynolds number on the dimensionless head-flow curve in this range of

Re is small, albeit Re is varied only by a factor of 2 and has not yet reached the prototype Re. If we assume that the effect of Re is small and, as a result, apply one parabolic-curve fit to all the data points (excluding at 1,185 RPM), we find

$$C_H = a_2 C_Q^2 + a_1 C_Q + a_o, \quad (21)$$

where the constant a's are found to be a_2 = -5,423, a_1 = 20.66, and a_o = 0.1615. The reason for the parabolic fit is due to the expected square-loss in the hydraulic head and is apparently suggested by the data. The linear and cubic fits are also shown as the light grey lines in the plot for comparison.

Finally, if we define the hydraulic power coefficient as $C_{\dot{m}gH} := \dot{m}gH/(\rho\omega^3 d^5)$, we find

$$C_{\dot{m}gH} = C_Q C_H, \quad (22)$$

where $C_{\dot{m}gH}$ can be written in terms of C_Q via Eq. (21).

6. Prediction of The Prototype Pump Operating Speed

Figure 5 also shows the predicted prototype pump performance by also showing the scales of the prototype pump head-flow at the same speed as that of the model on the secondary x and y axes according to the scaling law, Eq. (19). This can also be seen in dimensionless form in Fig. 6. From both figures, it is obvious that we have not yet achieved the prototype-equivalent desired head-flow at point A when we run the pump at the design speed of 1,000 RPM.

In order to predict the required operating speed for the prototype pump operating at head-flow of point A, we employ the dimensionless head-flow curve and apply similarity scaling as follows. If we assume that the dimensionless head-flow curve does not depend on Re, i.e., $C_H = f(C_Q)$, then the dimensionless head-flow curve shown in Fig. 6 is *the* head-flow curve of this pump in this range of C_Q. We can then *trace* the operating point A of the *prototype* pump on the $C_H - C_Q$ plane by using the set of parametric equations

$$C_Q(\omega) = \frac{Q_{A,p}}{\omega d_{2,p}^3} \quad \text{and} \quad C_H(\omega) = \frac{gH_{A,p}}{\omega^2 d_{2,p}^2}, \quad (23)$$

where ω is the varying parameter, $Q_{A,p}$ and $H_{A,p}$ are the flow and head at point A of the prototype pump, and $d_{2,p}$ is the diameter of the prototype pump. The result is shown in Fig. 6. Theoretically, the points on this trace correspond to different possible similarity states of all possible pumps that have the diameter of size $d_{2,p}$ and that can operate at the prototype head-flow at A at the corresponding ω, not of the same similarity state. The intersection point of this trace with the dimensionless head-flow curve of this pump from measurement then gives the dimensionless co-ordinates (C_Q, C_H) of the operating point and the corresponding speed for this pump. The determination of the operating speed of the prototype as described is basically the application of the similarity scaling law between the model and the prototype *at* the intersection point.

In this case, the result predicts that in order to achieve the desired flowrate and head at A, we need to operate the prototype at 1,185 RPM, approximately 20% above the design speed. This corresponds to C_Q = 2.73x10^{-3}, C_H = 0.177, and ω_s = 0.191, and the parameters of

the prototype (not model) of Re = 1.4x10^5 and K = 1.03x10^6 Pa-s^2/m^3.

Finally, while $C_H - C_Q$ curve is relatively independent of Re, at least within the current range of parameters, our preliminary result suggests that the efficiency depends more strongly on Re; the lower the Re, the lower the efficiency.

7. Test of The Prediction

In order to test the prediction from the dimensionless head-flow curve and similarity scaling law as described in Sec. 6, we proceed to make one additional test of the model at the same predicted speed for the prototype, i.e., 1,185 RPM. The dimensional and dimensionless test results are shown in Figs. 5 and 6, respectively. As is obvious from Fig. 5, we now achieve the prototype-equivalent desired head-flow at A for the *model* and, if the dimensionless head-flow curve is Re independent down to the prototype Re, also for the *prototype*. In addition, the dimensionless data points also collapse nicely onto the dimensionless head-flow curve from previous speeds, Fig. 6. This additional test therefore,

- confirms the similarity scaling between this model operating at different speeds, and
- further extends the validity of the dimensionless head-flow curve for this pump as described by Eq. (21) to a little higher Re; in other words, confirms the Re-independence assumption in this range of Re. In fact, after this test we also make one more test at the speed of 1,300 RPM, and the result still confirms the validity of the dimensionless head-flow curve nicely.

Table 2 summarizes some of the important parameters from the initial design of the prototype, the model tests, and the predicted performance of the prototype after incorporating the results of the model tests.

Table 2. Summary of important parameters.

	Designed Prototype	Model	Model	Predicted Prototype
Fluid	Blood	Water	Water	Blood
N (RPM)	1,000	1,000	1,185	1,185
Q (L/min)	5.8	39.2	46.4	5.8
H (m of fluid)	1.2	3.4	4.8	1.2
ω_s	0.162	0.191		
C_Q	3.24x10^{-3}	2.73x10^{-3}		
C_H	0.249	0.177		
Re	1.2x10^5	2.3x10^6	2.7x10^6	1.4x10^5
K (Pa-s^2/m^3)	1.2x10^6	4.9x10^5		1.03 x10^6
η (%)	100	27.4	38.4	?
$\dot{m}gH$ (W)	1.2	21.9	36.4	1.2

- Except Re and η, the values in the model columns are calculated from similarity at the intersection point of the measured dimensionless head-flow curve and the trace of the operating point A in Fig. 6; i.e., C_Q=2.73x10^{-3} and C_H=0.177.
- The efficiency η for the model columns are interpolated from the measured data at C_Q=2.73x10^{-3}.

When compare the point of maximum efficiency (mentioned in Sec. 5, η = 29.8%) and the similarity point (η = 27.4%) to the desired operating point at 1,000 RPM of the model in Table 2, we see that while the desired operating point is not the point of maximum efficiency, it is close. Its efficiency is lower than the maximum efficiency by approximately 10% of the maximum efficiency value. When compare the efficiencies at the same similarity state (same C_Q and C_H, models at 1,000 and 1,185 RPM) but different Re, we see that the efficiency depends on Re. Finally, since the efficiency depends on Re, we

make no prediction of the efficiency for the predicted prototype at this point.

8. Summary and Conclusion

In this work, the design scheme for a centrifugal blood pump based on 'one-dimensional' Euler's turbomachine equations is devised; the design is conducted; and a model is manufactured and tested. The resulting geometric parameters from the design are summarized in Table 1. In order to test the design at this early stage, a 2X scale-up model is used and the Re independence in the similarity scaling law is assumed. The model is then tested at the design prototype speed of 1,000 RPM, which corresponds to Re = 2.3×10^6, approximately 20 times higher than that of the prototype which is at 1.2×10^5. The model test result at this single Re shows that the actual total hydraulic head is about 70% of the ideal value and the maximum efficiency is 29.8%, and the designed pump cannot yet achieve the desired head-flow.

In order to predict the required operating speed of the prototype to operate at the desired head-flow at A, the effect of Re and Re dependence is then investigated. Additional tests are consequently conducted with the Re range extended down to $1.4\text{-}2.5 \times 10^6$ (600-1,100 RPM), but not yet reach the prototype Re. It is found that the dimensionless head-flow curve, given by Eq. (21), is independent of Re in this range. This dimensionless head-flow curve is then used to predict the required operating speed of the prototype; and the prediction gives the speed of 1,185 RPM, approximately 20% higher than the design value.

In order to test the prediction, the model is then tested at this predicted speed of the prototype. The test confirms the prediction; and, the model achieves the prototype-equivalent desired head-flow at A. In another aspect, the test confirms the similarity scaling law for the model operating at different speeds and, together with another test at 1,300 RPM, extends the validity of Re-independence dimensionless head-flow curve of this pump to Re $1.4\text{-}2.9 \times 10^6$.

Finally, the performance parameters of the prototype, after incorporating the more realistic data from the model testing, are predicted and given in the last column of Table 2. It is concluded that if the dimensionless head-flow curve of this pump is independent of Re down to the prototype Re, the prototype should be able to deliver the desired head-flow at A successfully at 1,185 RPM. The remaining issue is then whether the assumption of Re independence down to the prototype Re is valid.

9. Acknowledgement

This project is funded by Stimulus Package 2 (SP2) of Ministry of Education under the theme of Green Engineering for Green Society. The authors also would like to thank the Head of The Mechanical Engineering Department, Aj. Chinatep Benyajati, and Aj. Somsak Chaiyapinunt who initiate and support the project, and to Aj. Werayut Srituravanich who helps managing the funding. They also greatly appreciate Dr. Takashi Yamane's visit and presentation. They would like to thank also Mr. Kitipong Kangvanskol for his help in conducting some of the tests.

10. References

[1] Thoractec. URL: http://www.thoratec.com/medical-professionals/vad-product-information/index.aspx

[2] Jarvik Heart. URL: http://www.jarvikheart.com/home.asp.

[3] HeartWare. URL: http://www.heartware.com.au/IRM/content/usa/products_HVAD.html.

[4] Levitzky, M. G., 1997. Cardiopulmonary Physiology in Anesthesiology, McGraw-Hill, New York.

[5] Gülich, J. F., 2010. Centrifugal Pumps, Second Edition, Springer, Berlin.

[6] EBARA Corporation, 2001. The EBARA Pump System Engineering Handbook, EBARA Corporation.

[7] Yamane, T., Maruyama, O., Nishida, M., Kosaka, R., Sugiyama, D., Miyamoto, Y., Kawamura, H., Kato, T., Sano, T., Okubo, T., Sankai, Y., Shigeta, O., and Tsutsui, T., 2007. Hemocompatibility of a hydrodynamic levitation centrifugal blood pump, J. Artif Organs, Vol. 10, pp. 71–76.

[8] Yamane, T., 2010. Implantable Non-pulsatile Artificial Heart - Study with flow visualization, Thailand-Japan Workshop, Nov. 17, 2010, Chulalongkorn University, Bangkok.